Chapter 4:
Compound defect in BP for enhanced gas sensing

4.1 Introduction

Sensing of toxic gas molecules has been a subject of topical research, and black phosphorene (BP) with its high surface to volume ratio, vast reaction sites, high chemical activity, and quality charge transfer between the surface and molecules, have shown promising results in sensing and storing toxic gases [1–5]. It has been confirmed that pristine BP has strong sensing abilities that are even more potent than those of graphene and MoS_2. As reported by Kou *et al.*, the adsorption energies of CO, CO_2, NH_3, NO, and NO_2 on pristine BP are significantly higher than their adsorption energies on graphene and MoS_2 [6]. Besides, when physisorbed by small molecules, BP undergoes electronic polarization, making it highly suitable for sensing these molecules [7–9]. Reports also suggest that pristine BP has good adsorption energies for SO_2 and nitrogen-based (NH_3, NO_2) gas molecules [7,10]. In an empirical study for the chemical detection of NO_2, field-effect transistors based on layered black phosphorus performed effectively and efficiently, when compared to alternative sensors, such as monolayer MoS_2 [11].

Thus, in comparison to other two-dimensional (2D) materials, BP is an excellent candidate for nanosensor devices. However, as discussed in Chapter 3, BP is prone to defects and is likely to form compound defect within it. Defects can be considered as an advantageous characteristic as they are widely recognized for their ability to fine-tune the surface reactivity and chemical selectivity of 2D materials. For instance, BP has demonstrated excellent responsiveness for detecting nitrogen-based gases when doped with non-metallic N, S, and O. BP doped with metallic elements also promotes NO adsorptions [1,3,12]. Therefore, building on the discussion of compound defect in Chapter 3, in this chapter we explore the surface adsorption of five environmentally detrimental gas molecules, namely NO_2, SO_2, CO, CO_2, and NH_3, on BP with a compound defect. To identify the most influential defect, we also explore how each of the point defects (i.e., vacancy and the dopant) affects surface adsorption independently. The monolayers with a compound defect (BP_V^N), a P vacancy (BP_v), and a doped N (BP^N) are shown in Fig. 4.1(a-c).

4.2 Computational details

The optimised structures of pristine BP, BP_v, BP^N, and BP_V^N discussed in Chapter 3 are used to introduce the gas molecules for surface adsorption. The surface structures are treated with Projector-augmented waves (PAWs) pseudo potentials within a dense

Monkhorst *k*-grid of 6×1×6 and 12×1×12 was used for the self-consistent field and non-self-consistent field calculations respectively [13–16]. Perdew-Burke-Ernzerhof (PBE) exchange-correlation functional with generalised gradient approximation (GGA) was considered for all the calculations [17]. The values of kinetic energy cutoff and charge density cut off were set to 50 Ry and 300 Ry, respectively. The structures were allowed to relax until a force convergence threshold of 10^{-3} Ry/Bohr was achieved. The convergence criteria for the self-consistent calculations were chosen to be 10^{-6} Ry for all the modelled structures. The calculations were carried out using QUANTUM ESPRESSO software package [18,19].

4.3 Surface adsorption

One of the most beneficial flaws of BP is creation and utilization of vacancies [20–22]. Introducing a single P vacancy causes the Fermi level to drop down slightly below the valence band, making BP_v a p-type semiconductor. Consequently, the decrease in coordination number of the P atoms in the vicinity of the vacant site generates unpaired electrons, forming a dangling bond and inducing a magnetic moment of 0.84 μ_B in the system, consistent with the previous study [23]. The BP^N layer also behaves as a p-type semi-conductor, but exhibits no magnetism (0.02 μ_B) since the substituted N atom has the same number of valence electrons as P [24].

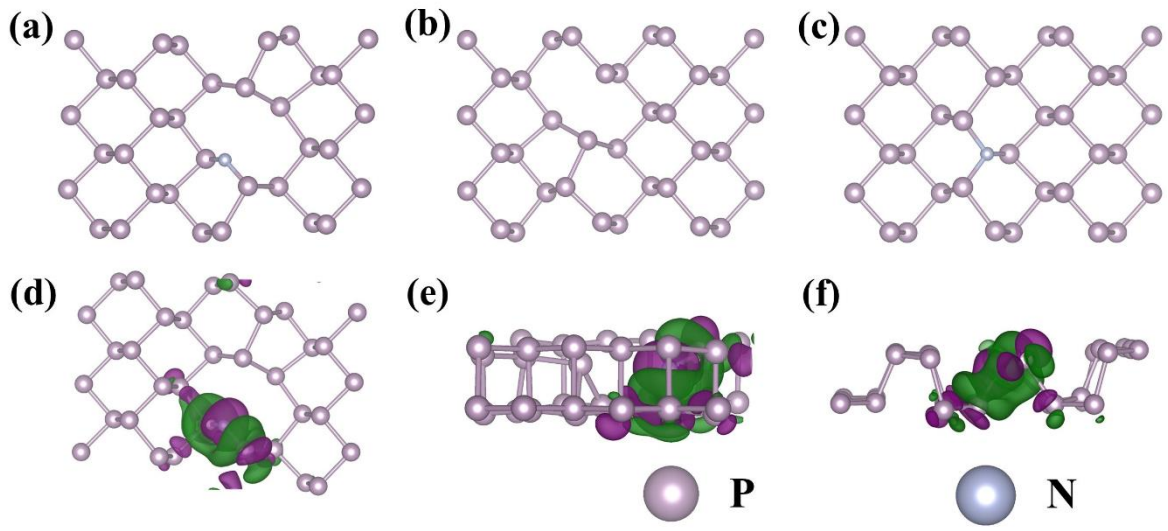

Figure 4.1: *Relaxed structures of (a) BP_v^N, (b) BP_v, and (c) BP^N sheet; (d) top view and (e, f) side view of charge density difference in BP_v^N sheet (note that the region in green and purple represents accumulated and depleted charged regions, respectively).*

When a foreign N atom is present with a P vacancy in BP_v^N sheet, the magnetic moment is slightly altered, giving 0.08 μ_B ($\approx 0\,\mu_B$). Thus, the presence of N compensates for the magnetic moment induced by the P vacancy. The induction (non-induction) of magnetic moment can be visualised by the asymmetries (symmetries) between the spin up and spin down states of the layers close to the Fermi level, as discussed in chapter 3 (Fig. 3.5, and Fig. 3.6).

The work function (WF) of a material defines the minimum energy required to remove an electron from its surface and is calculated as the difference between the vacuum level and the Fermi level. For BP_v and BP^N, the WFs are 0.90 eV and 1.39 eV, respectively. This indicates that a higher interaction energy is needed to remove an electron from the BP surface containing a phosphorus vacancy. Since the compound defect also involves a vacancy, the WF of the BP_v^N surface is found to be 1.57 eV. The details of the WF calculation are shown in Appendix A.1.

It is apparent that the p-type nature of BP_v and BP^N brought on by the vacancy and the dopant, respectively, is retained by their combination in BP_v^N. As an enhancement, the layer becomes more interactive and chemically reactive towards NO_2, and SO_2 molecules owing to the structural deformation caused by the sharp variations in P-P distances, and also a lowering in the coordination number. To understand and analyse the nature, and sensing behaviour of adsorption, it is essential to investigate the behaviour of the electronic states and the amount of charge transferred between the layer and the adsorbed molecule. Due to the induced magnetism, spin polarised calculations are carried out for the BP_v layer to comprehend the alterations in the electronic states.

The minimum distance, *d*, between the atoms of the adsorbed molecule and the layer is calculated from the most stable optimized configurations (Table 4.1). If this distance is smaller than the sum of the covalent atomic radii ($r_{cA} + r_{cB}$) of two atoms (A and B), the molecule is characterized as chemisorbed onto the layer. In contrast, physisorption happens when the separation distance surpasses the total of the covalent atomic radii of the two atoms sharing the minimal contact [25,26]. A schematic illustration of chemisorption and physisorption behaviour of gas molecules on BP_v^N surface is shown in Appendix A.2. A smaller value of *d* indicates stronger adsorption to the site under consideration. In addition, the calculated electron localisation function (ELF) of the adsorbed structures also provides significant information about the nature of the bond and type of adsorption. To be

mentioned, a large difference in electronegativity between the atoms also reflects higher adsorption energy. Strong adsorption energies illustrate the strong binding between the layer and the molecule, serving as a cause for the charge transfer events. This process results in an eventual disparity in electrical conductivity. As a result, the contrast in charge manifestations and consequently, surface conductivity determines the sensitivity. Theoretically, the adsorption energy reflects the fundamental process of charge transfer in conjunction with the bonding between the atoms of the layer and the molecule. The negative adsorption energy (E_{ad}) for all the molecules showed that the reactions are exothermic in nature. Furthermore, to clearly understand the role of uneven distribution of charge densities arising due to the compound defect, the charge density difference (CDD) is also plotted. Figure 4.1(d-f) depicts the distribution of charge accumulation/depletion concentrating near the site of the compound defect. The accumulation near the N is a result of the higher electronegativity of the atom than that of P.

To determine the strength of the adsorption process of the gas molecules on the different layers, adsorption energies are calculated using the following formula-

$$E_{\text{ad}} = E_{(\text{layer+gas})} - E_{(\text{layer})} - E_{(\text{gas})} \quad \ldots(4.1)$$

where, $E_{(\text{layer+gas})}$, $E_{(\text{layer})}$, and $E_{(\text{gas})}$ are the total energy of defected BP layers with the adsorbed gas molecule, without the gas molecule, and the isolated molecule, respectively. For an exothermic reaction, the adsorption energy from equation (4.1) should be negative (E_{ad}<0). Further, charge transfer between the adsorbed molecules and the BP surfaces is attained using Bader charge analysis [27]. In addition, the charge density difference (CDD) is also obtained using the formula-

$$\Delta\rho = \rho_{(\text{layer+gas})} - \rho_{(\text{layer})} - \rho_{(\text{gas})} \quad \ldots(4.2)$$

where, $\rho_{(\text{layer+gas})}$, $\rho_{(\text{layer})}$, and $\rho_{(\text{gas})}$ are the total charge densities of layers with the adsorbed molecule, without the adsorbed molecule, and an isolated gas molecule; respectively. It is to be mentioned that different orientations of the gas molecules were considered, and the surface adsorption phenomena were analysed based on the most stable configuration, corresponding to the highest negative E_{ad} value. The E_{ad} values for different orientations are provided in Appendix A.3.

Table 4.1: Adsorption energy (E_{ad}), charge transferred (ΔQ) between the layer and the molecule, minimum distance (d) between the atoms of the layer and the molecule (closest atoms are mentioned within the brackets), and the nature of adsorption of NO_2, SO_2, CO, CO_2, and NH_3, molecules.

Target	Surface of adsorption	E_{ad} (eV)	ΔQ (e)	d (Å) (A-B)	Type of adsorption	Recovery time (s)
NO_2	BP	-0.42	0.116	2.77 (P-O)	Physisorption	1.04×10^{-6}
	BP_v^N	-5.74	1.000	1.52 (P-O)	Chemisorption	7.57×10^{82}
	BP_v	-4.40	1.351	1.61 (P-O)	Chemisorption	3.13×10^{60}
	BP^N	-0.51	0.310	2.71 (P-O)	Physisorption	3.30×10^{-5}
SO_2	BP	-0.43	0.169	2.90 (P-O)	Physisorption	1.52×10^{-6}
	BP_v^N	-0.13	0.129	3.12 (P-S)	Physisorption	1.48×10^{-11}
	BP_v	-0.03	0.011	3.71 (P-O)	Physisorption	3.17×10^{-13}
	BP^N	-0.07	0.045	3.48 (P-O)	Physisorption	1.48×10^{-12}
CO	BP	-0.13	0.045	3.17 (P-O)	Physisorption	1.48×10^{-11}
	BP_v^N	-0.02	0.010	3.99 (N-C)	Physisorption	2.16×10^{-13}
	BP_v	-0.02	0.010	3.79 (P-C)	Physisorption	2.16×10^{-13}
	BP^N	-0.05	0.010	3.69 (P-C)	Physisorption	6.84×10^{-13}
CO_2	BP	-0.19	0.049	3.28 (P-O)	Physisorption	1.49×10^{-10}
	BP_v^N	-0.05	0.015	3.82 (P-O)	Physisorption	6.84×10^{-13}
	BP_v	-0.03	0.014	3.75 (P-C)	Physisorption	3.17×10^{-13}
	BP^N	-0.05	0.013	3.72 (P-O)	Physisorption	6.84×10^{-13}
NH_3	BP	-0.29	0.124	3.07 (P-H)	Physisorption	6.98×10^{-9}
	BP_v^N	-0.03	0.003	3.41 (P-H)	Physisorption	3.17×10^{-13}
	BP_v	-0.03	0.006	3.20 (P-H)	Physisorption	3.17×10^{-13}
	BP^N	-0.05	0.002	3.28 (P-H)	Physisorption	6.84×10^{-13}

4.3.1 Surface adsorption of NO_2

Since NO_2 is a paramagnetic molecule, spin polarized calculations are essential to carry out its adsorption behaviour on the surfaces before and after adsorption. Under the combined effect of N doping and P vacancy, the molecule is strongly chemisorbed onto the BP_v^N surface, as the minimum distance of separation, 1.52 Å, is less than the sum of the covalent atomic radii of P-O atoms (typically, 2.74 Å) (Fig. 4.2(a)). The chemical bonding

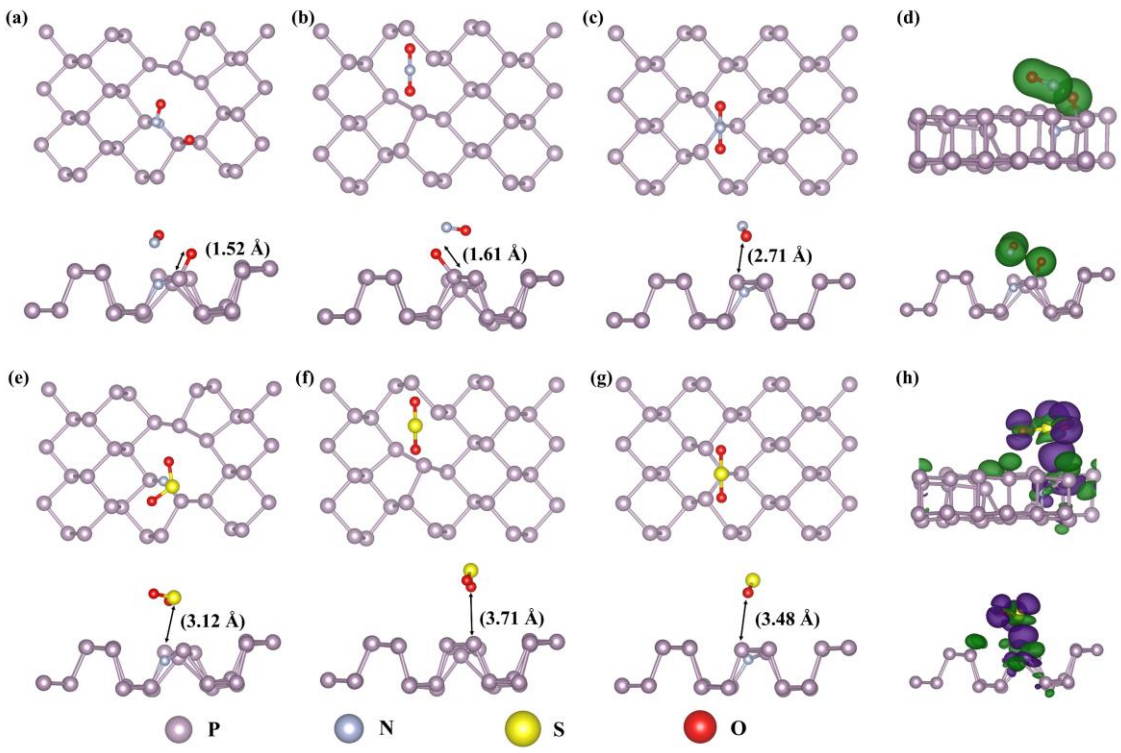

Figure 4.2: *Relaxed structures of adsorbed (a-c) NO_2 and (e-g) SO_2 on BP_v^N, BP_v, and BP^N surface, respectively. Charge density difference of BP_v^N after adsorption of (d) NO_2, and (h) SO_2 molecules (purple regions represent the depletion and green regions represents an accumulation of charges).*

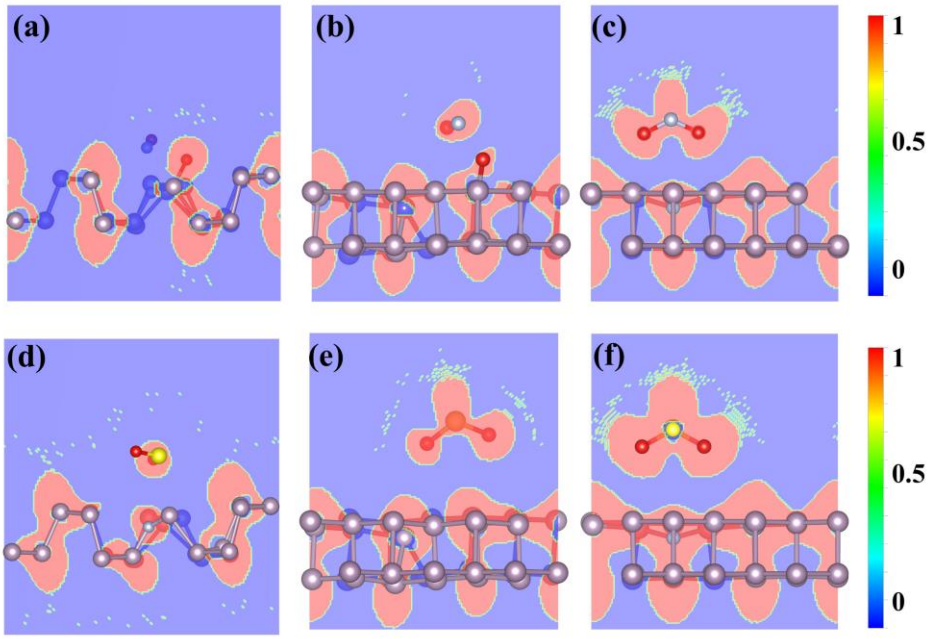

Figure 4.3: *Electron localisation function (ELF) plots of (a-c) NO_2, and (d-f) SO_2 on BP_v^N, BP_v, and BP^N surfaces, respectively.*

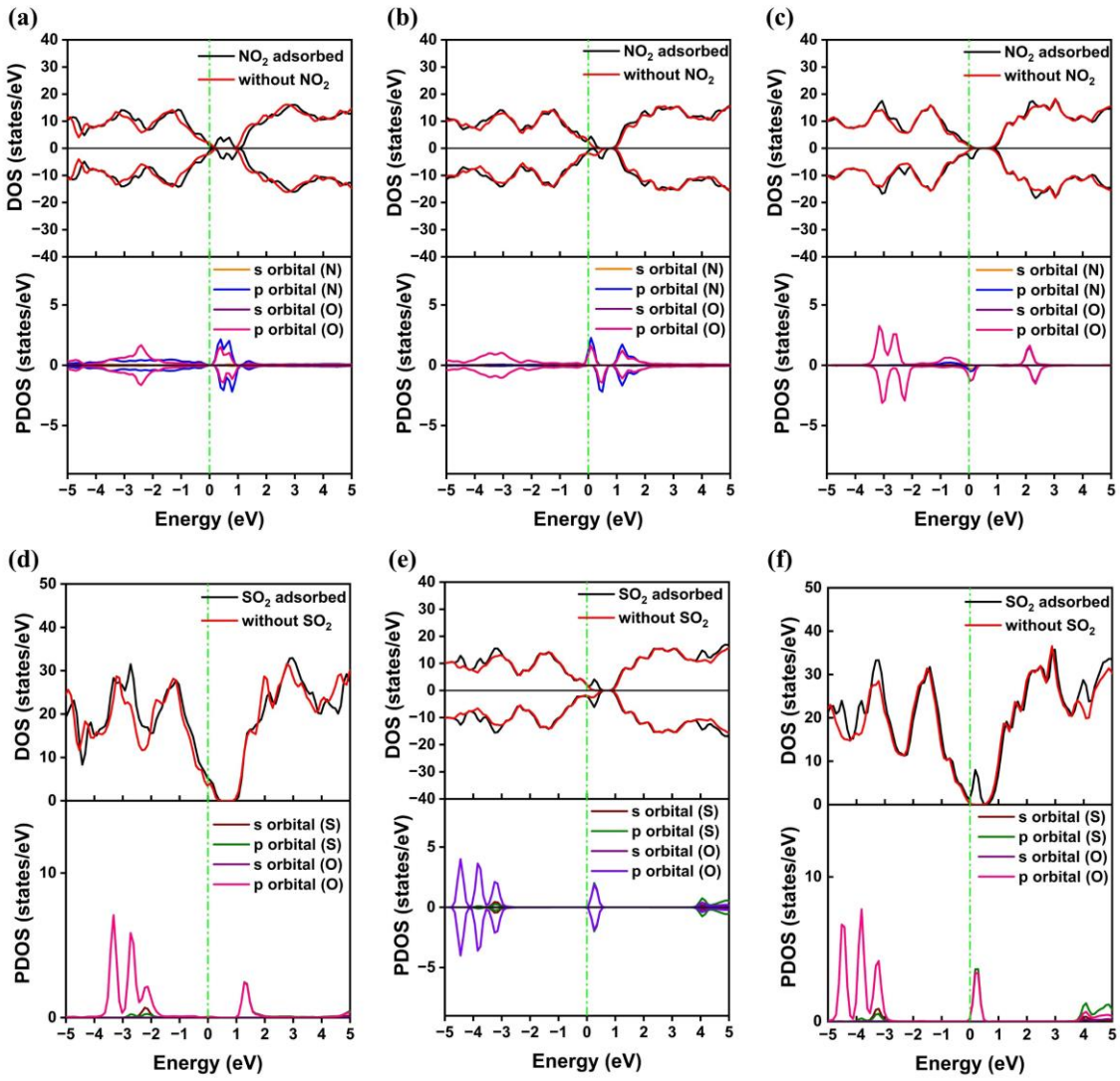

Figure 4.4: *DOS (upper stack) and projected DOS (lower stack) of* BP_v^N*,* BP_v*, and* BP^N *sheet before and after adsorption of (a-c)* NO_2*, and (d-f)* SO_2 *molecules, respectively (red and black colour indicates DOS before and after adsorption; dark yellow and purple colour indicates s orbital, pink and violet colour indicates p orbital of N and O atom, respectively).*

between the P and O atoms can also be visualised from the ELF plot (Fig. 4.3(a)). As compared to pristine BP, a drastic increase in the value of adsorption energy is observed in BP_V^N monolayer. With a highly negative adsorption energy, the strong chemisorption process causes an N-O bond within the molecule to get broken. The detached O atom sits at a distance of 2.29 Å from the parent molecule and bond with a P atom, which lie next to the vacant site. This robust attraction is reflected in the high adsorption energy (-5.74 eV) of BP_V^N towards the molecule. Bader charge analysis shows that charge equivalent to an

electron is transferred from the layer to the molecule, indicating an ionic bond formation between the layer and the molecule. It also reveals that the doped N atom loses 1.22 e charge after the adsorption of the NO_2 molecule, pointing out to its strong contribution in the chemisorption. The chemical bonding between the O atom of the molecule with the P atom of the host surface can be visualised from the ELF plot shown in Fig. 4.3(a). Moreover, the DOS plot reveals elimination of the energy band gap and induction of magnetic moment into the system, attributed to the asymmetric impurity states near the Fermi level (Fig. 4.4(a) upper stack). According to projected density of states (PDOS), the asymmetric states near the Fermi region are localised at the 2*p* orbitals of N and O atoms (Fig. 4.4(a) lower stack). From the CDD of NO_2, accumulation of negative charges around the three atoms of the molecule clearly signifies that a high amount of charge has been transferred to the molecule (Fig. 4.2(d)).

Next, we delve into the adsorption of the NO_2 molecule on BP_v and BP^N layers to discern the primary defect influencing chemisorption under the influence of their combination. Based on the distance of separation, it can be concluded that the molecule is chemisorbed on the BP_v layer, while the nature of adsorption in BP^N leans towards physisorption (Fig. 4.2(b,c)). Analogous to BP_v^N, in BP_v, the detachment of the O atom under the effect of single P vacancy makes the desorption improbable (Fig. 4.2(b)). The adsorption energy and charge transfer for BP_v system are -4.40 eV and 1.351 e, whereas it is -0.51 eV and 0.310 e for BP^N (Table 4.1). Even though BP_v^N and BP_v surfaces possess higher WF compared to BP^N, the higher charge transfer in the two surfaces is fuelled by the very strong interaction with the NO_2 molecule. Consequently, it is speculated that the robust chemisorption of BP_v^N towards NO_2 can be attributed to the presence of a P vacancy in the system, suggesting that a BP system with vacancies can function as a storage for NO_2 molecules. The chemisorption and physisorption of NO_2 on BP_v^N, and BP_v is also evident from the ELF plots shown in Fig. 4.3(b,c). Comparing the electronic states of BP_v and BP_v^N, less impurity peaks are observed near the Fermi level in BP^N (Fig. 4.4(a-c)). This, coupled with the relatively lower charge transfer and adsorption energy, suggests that controlled growth of vacancies in an N-doped BP can make it a promising sensor for NO_2 molecules. In all three systems, the direction of charge transfer is from the layer to the molecule, a consequence of the higher electronegativity of the O atom in comparison to P, as they share the minimum distance.

4.3.2 Surface adsorption of SO_2

After adsorption, the SO_2 molecule sits at a distance of 3.12 Å from the BP_v^N layer, as depicted in Fig. 4.2(e). The nature of adsorption in this case is physisorption, as the distance between the molecule and the layer surpasses the sum of the covalent atomic radii of P-S (typically 2.40 Å). The physisorption nature of bonding can be visualised from the ELF profile shown in Fig. 4.3(d). Examining the electronic states, the DOS of BP_v^N reveals an intricate pattern. Around the Fermi level, between 0 eV and 1.5 eV, the electronic states in conduction band remain unchanged (Fig. 4.4(d) upper stack). Away from the Fermi level, the valence band displays notable changes in DOS, with visible impurity peaks at -2.70 eV. The impurity states in the conduction band, away from the Fermi level, have minimal impact on the electronic structure. Analysing the PDOS of the SO_2 molecule, it is apparent that the impurity states originate from the 2*p* orbitals of the two O atoms on both sides of the Fermi level, as shown in the lower stack of Fig. 4.4(d). However, we observe slight differences in the valence band states near the Fermi level after adsorption. This change does not originate from the external molecule but rather from the orbitals of the host atoms. Charge depletion on the surface of the BP_v^N and accumulation surrounding the atoms of the molecule is visible in Fig. 4.2(h). With an adsorption energy of around -0.13 eV, this interaction functions as a sensitive sensor of SO_2, supported by a charge transfer of 0.129 e. However, in comparison to the adsorption of SO_2 on pristine BP, both the adsorption energy and charge transfer have decreased by -0.3 eV and 0.040 e, respectively (Table 4.1).

Moving forward, the investigation explores the adsorption of SO_2 on BP_v and BP^N layers, assessing if a single point defect retains the sensing capability of the combined defect (Fig. 4.2(f,g)). Nevertheless, the adsorption energy and charge transfer in both layers decrease to -0.07 eV, 0.045 e (BP^N), and -0.03 eV, 0.011 e (BP_v), reducing the sensitivity offered by the combinatorial effect. While some noticeable changes occur near the Fermi level of BP_v, and the BP^N sheet after adsorption, these alterations prove insufficient to compensate for the decline in adsorption energy and charge transfer, essential factors for the layers to function effectively as sensors (Fig. 4.4(e,f)). Charge transfer direction in all three systems is from the layer to the molecule, dictated by the higher electronegativity of the S and O atoms in the molecule.

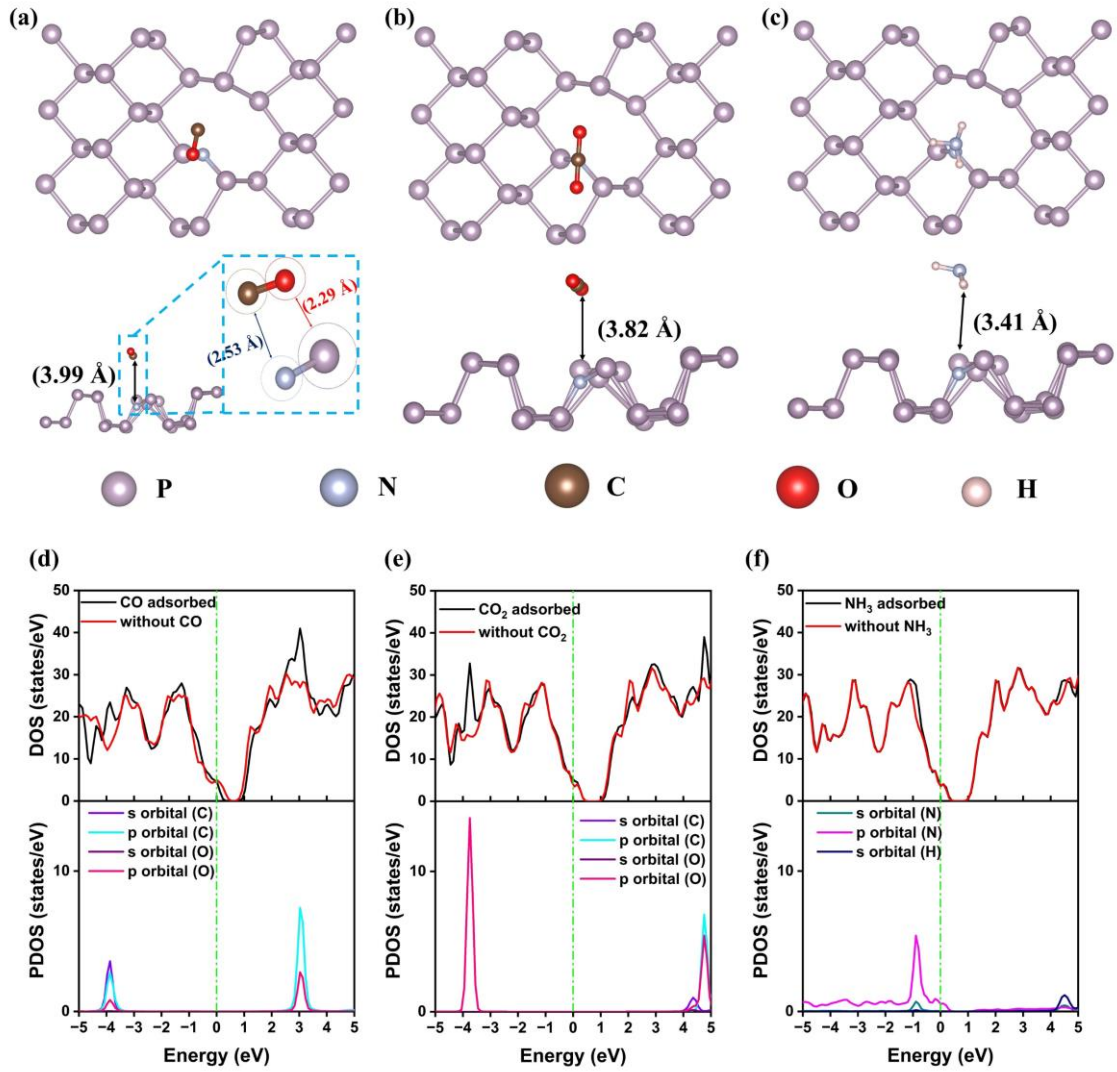

Figure 4.5: *Relaxed structures and DOS of BP_v^N sheet after (a,d) CO, (b,e) CO_2, and (c,f) NH_3 adsorption, respectively (red and black colour indicates DOS before and after adsorption; dark yellow and purple colour indicates s orbital, pink and violet colour indicates p orbital of N and O atom, respectively).*

4.3.3 Surface adsorption of CO, CO_2, and NH_3

Compared to pristine BP, under the effect of combined point defects, BP_v^N layer remains impervious towards CO, CO_2, and NH_3 molecules with very low adsorption energies and charge transfer (Table 4.1). For CO molecule, the C atom relaxes directly above the doped N atom to share the minimum distance, while for CO_2, it is the O atom sharing the minimum distance with the P atom next to the doped N (Fig. 4.5(a,b)). As for NH_3, the H atom shares the minimum distance with the nearest P atom of the BP_v^N layer (Fig. 4.5(c)). The DOS of BP_v^N with these adsorbed molecules reveals an absence of impurity peaks near

the Fermi level, but shows small impurity peaks away from the Fermi level, owing to the very weak physisorption nature of adsorption (Fig. 4.5(d-f)). Consequently, the BP layer with combinatorial defects demonstrates insensitivity towards these molecules.

Additionally, investigations into the adsorption of these molecules on both BP_v and BP^N layers, aiming to evaluate potential enhancements in adsorption due to the presence of a single vacancy, yielded consistent results (Fig. 4.6(a-f)). The adsorption energy and charge transfer values showed no noticeable change compared to BP_v^N, emphasizing the insensitivity of these systems towards the molecules (Table 4.1). This insensitivity is further confirmed by the absence of additional peaks in the electronic structure of the adsorbed surfaces (Fig. 4.7(a-f)). Furthermore, ELF plots for the adsorption of these molecules indicate weak interactions with the surfaces (Fig. 4.8(a-f)). Notably, the charge

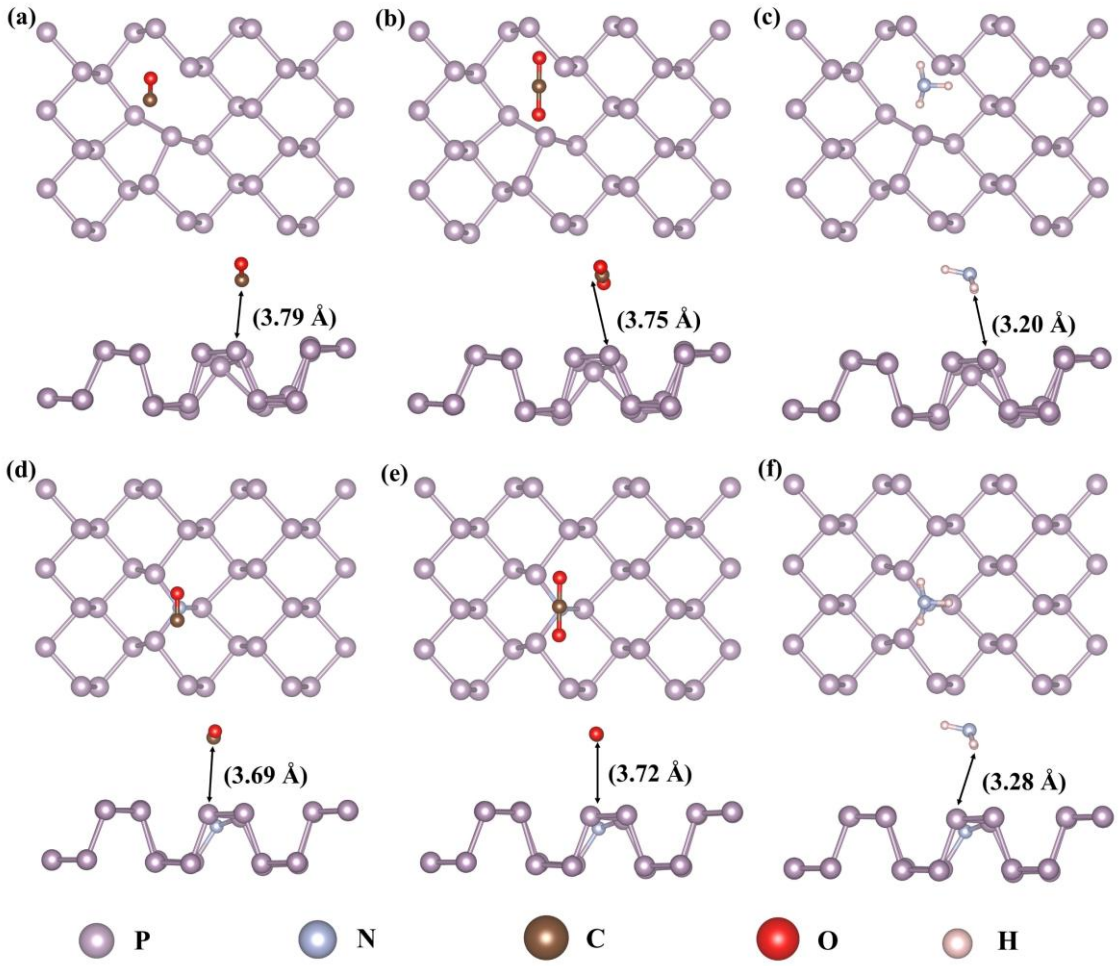

Figure 4.6: *Relaxed structures of BP_v, and BP^N sheet after (a,d) CO, (b,e) CO_2, and (c,f) NH_3 adsorption, respectively.*

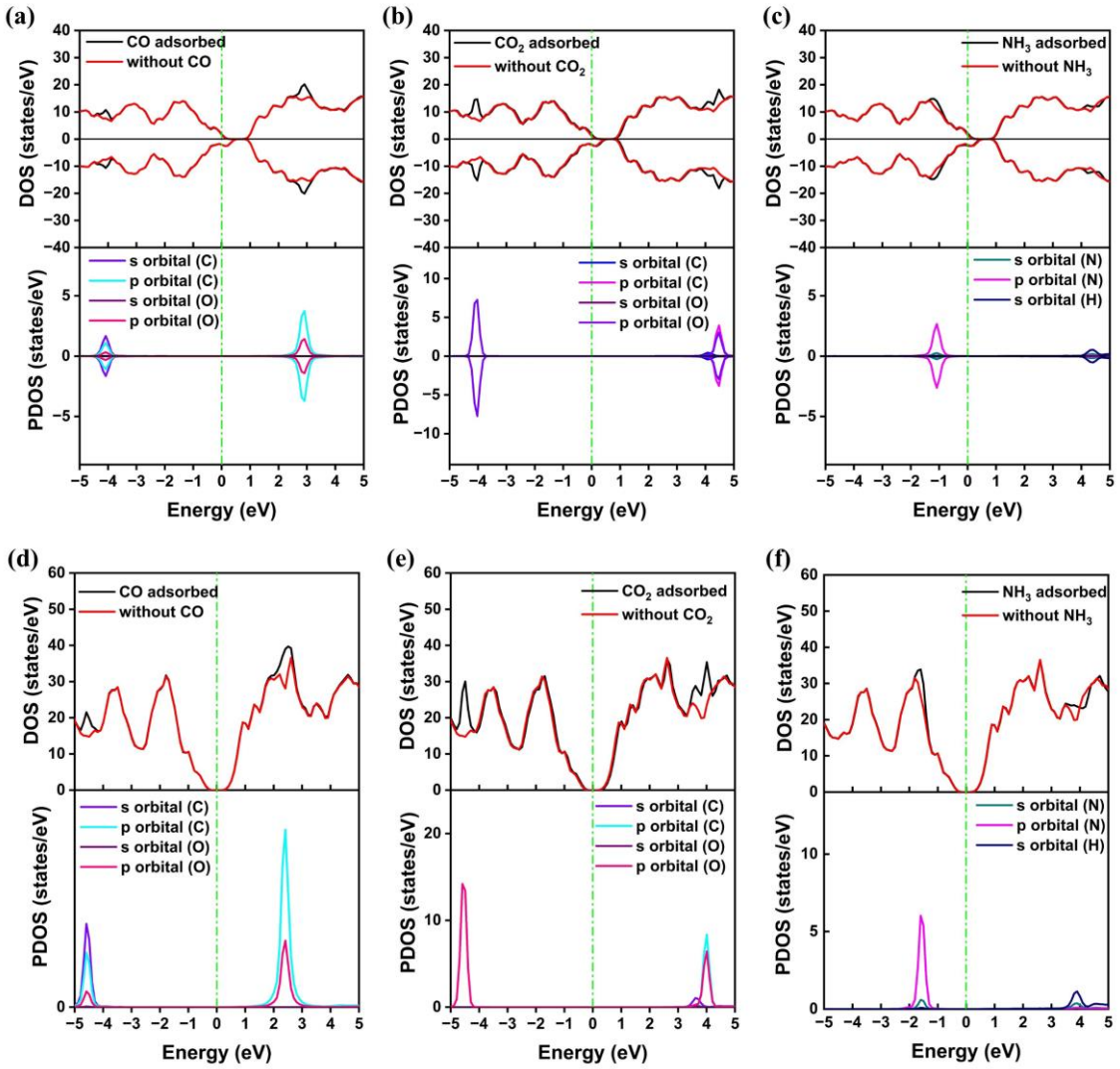

Figure 4.7: *DOS (upper stack) and projected DOS (lower stack) of BP_v, and BP^N sheet before and after adsorption of (a,d) CO, (b,e) CO_2, and (c,f) NH_3 molecules, respectively (red and black colour indicates DOS before and after adsorption; dark yellow and purple colour indicates s orbital, pink and violet colour indicates p orbital of N and O atom, respectively).*

transfer direction in all systems is from the layer to the molecule. The direction of charge transfer is governed by the higher electronegativity of the two atoms sharing the minimum distance. It is known that the electronegativity of the atoms follows the order P<H<C<S<N<O. The charge transfer between BP_v^N and CO seems contradictory as the electronegativity of N is more than that of C. But it can be explained through the interaction between the next closest atoms (P-O) of the layer and the molecule. After adsorption, P and O atoms sit at a distance of 4.03 Å apart from each other. The outer shell electrons of

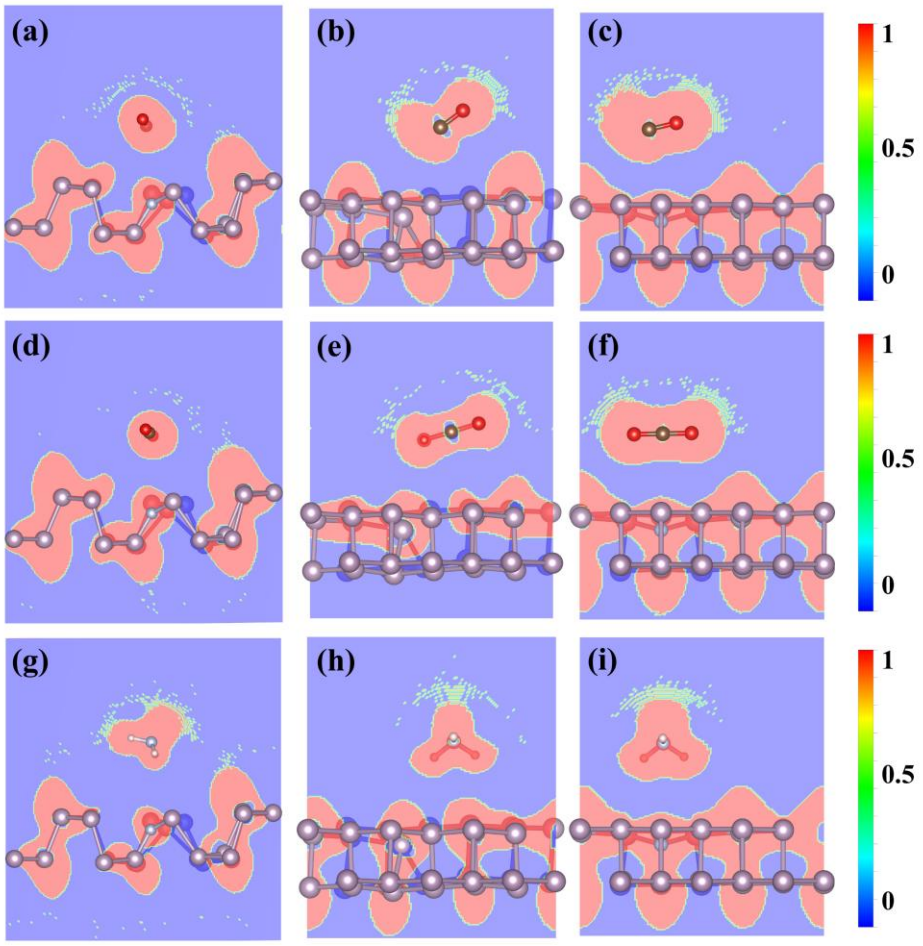

Figure 4.8: *Electron localisation function (ELF) plots of (a-c) CO, (d-f) CO_2, and (g-i) NH_3 on BP_v^N, BP_v, and BP^N surfaces, respectively.*

P and O are closer to each other than those of N and C atom (shown in the bottom right of Fig. 4.5(a) as an inset). Thus, the charge transfer from the layer to the molecule is due to the difference in electronegativity between the P and O atom. The low E_{ad} values and charge transfer for NH_3, despite a less distance from the layers as compared to that of CO, and CO_2 can be explained through the smaller covalent atomic radii of H atom. It is to be mentioned that the changes in electronic states of the host layers after adsorption of CO, CO_2, and NH_3 is very little, and occurs away from the Fermi level. Thus, BP_v^N, BP_v, and BP^N layers are found to be insensitive towards these three molecules.

4.3.4 Recovery time

The typical timescale, denoted as τ for an elementary reaction can be estimated using the Van't-Hoff-Arrhenius equation for the rate constant. Thus, according to transition state

theory, recovery time (τ) for monolayers to desorb molecule can be expressed as follows [28,29]

$$\tau = \omega^{-1}\exp\left(\frac{|E_{ad}|}{K_B T}\right) \quad \ldots(4.3)$$

Here, ω represents the attempt frequency. K_B, and T are the Boltzmann's constant and temperature respectively. As per transition state theory, the factor ω falls within the order of magnitude 10^{13} s^{-1} [28,29]. At a temperature T= 300 K, the value of K_BT is approximately 0.026 eV.

In the case of NO_2 molecule, the BP_v^N, and BP_v monolayers exhibit exceptionally high adsorption energy, leading to such a strong interaction that the molecule undergoes breakage. Consequently, desorption within these layers appears nearly impossible, with recovery times estimated at 10^{82} s and 10^{60} s (Table 4.1). The relatively swift recovery time of 3.30×10^{-5} s for the BP^N monolayer suggests its potential as a sensor for this molecule. For the SO_2 molecule, recovery time across BP_v^N, BP_v, and BP^N monolayers are in the range of 10^{-11} s to 10^{-13} s. However, it's worth noting that only the BP monolayer with compound defect exhibits favourable adsorption energy, indicating its effectiveness in sensing the molecule. As for CO, CO_2, and NH_3, their very low adsorption energy enables the desorption process within an incredibly short timeframe, typically around 10^{-13} s.

4.4 Conclusion

To conclude, a comprehensive study as regarding the adsorption phenomena of five distinct hazardous gas molecules on BP monolayers has been carried out, considering a compound defect. Our investigation, based on first-principles calculations, included changes in electronic properties, charge transfer, and CDD. Additionally, we examined the adsorption phenomena in a BP monolayer with a single-point defect to understand individual contribution from the point defects. Previous reports have highlighted that the existence of dangling bonds in BP can foster the creation of more robust bonds with NO_2 molecules [6]. Building upon this background, our current study provides additional insights, revealing that the NO_2 molecule indeed demonstrates a robust interaction with BP_v and BP_v^N layers. This interaction manifests in notable surface adsorption phenomena, consequently yielding high values of adsorption energy, specifically -4.40 eV and -5.74 eV, respectively. In both systems, the substantial chemical interplay between the outermost

orbitals of nitrogen and oxygen atoms of the molecule and the dangling bonds results in the elimination of the band gap and the breaking of the N-O bond in the molecule. Desorption of the NO_2 molecule from these two sheets is deemed non-viable, suggesting their potential use as storage for the molecule. Conversely, in the case of NO_2 adsorption on the BP^N sheet, the absence of dangling bonds weakens the interaction. This characteristic proves advantageous for the system to function effectively as a gas sensor for the molecule. Asymmetries in the electronic states of BP_v, BP^N, and BP_v^N after adsorption are attributed to the paramagnetic behaviour of the molecule. Pristine BP has also previously been acknowledged for its favourable adsorption energy towards SO_2 molecules [10]. In our investigation, both BP layers with single defects exhibit a weak interaction with the SO_2 molecule. However, when combining both defects in a single BP layer, there is a noticeable increase in adsorption energy and charge transfer of the layer towards the molecule. Consequently, it may be extrapolated that the BP_v^N layer, with the combination of defects, can still function as an effective sensor for SO_2 molecules, displaying a nearly equivalent amount of charge transfer as pristine BP [10]. Interestingly, the system with compound defect shows insensitivity towards CO, CO_2, and NH_3 molecules. The minimal change in electronic states near the Fermi level post-molecule adsorption suggests a weak adsorption process and weak chemical bonding. These outcomes align with the low charge transferred between the layer and the molecules, causing almost negligible changes in the charge carrier density of the monolayer after adsorption. Thus, it is evident that the presence of a vacancy in the BP sheet offers a pathway for the material to serve as a storage medium for NO_2 molecules. On the other hand, without a vacancy and upon doping with an N atom, it functions as a sensor for the molecule. The combination of defects in the BP_v^N sheet emerges as a unique approach to utilize the material as a sensor for SO_2 molecules.

References

[1] Suvansinpan, N., Hussain, F., Zhang, G., Chiu, C. H., Cai, Y., Zhang, Y. W. Substitutionally doped phosphorene: electronic properties and gas sensing. *Nanotechnology*, 27(6): 065708, 2016.

[2] Ye, H., Liu, L., Xu, Y., Wang, L., Chen, X., Zhang, K., Liu, Y., Koh, S.W. and Zhang, G. SnSe monolayer: A promising candidate of SO_2 sensor with high adsorption quantity. *Applied Surface Science*, 484: 33–38, 2019.

[3] Prasongkit, J., Shukla, V., Grigoriev, A., Ahuja, R., Amornkitbamrung, V. Ultrahigh-sensitive gas sensors based on doped phosphorene: A first-principles investigation. *Applied Surface Science*, 497: 143660, 2019.

[4] Li, Q., Liu, Y., Chen, D., Miao, J., Zhi, X., Deng, S., Lin, S., Jin, H. and Cui, D. Nitrogen dioxide gas sensor based on Ag-doped graphene: a first-principle study. *Chemosensors*, 9(8): 227, 2021.

[5] Zhang, H., Du, A., Shi, Q., Zhou, Y., Zhang, Y., Tang, Y. Adsorption behavior of CO_2 on pristine and doped phosphorenes: A dispersion corrected DFT study. *Journal of CO_2 Utilization*, 24: 463–470, 2018.

[6] Kou, L., Frauenheim, T., Chen, C. Phosphorene as a superior gas sensor: selective adsorption and distinct I–V response. *The journal of physical chemistry letters*, 5(15): 2675–2681, 2014.

[7] Cai, Y., Ke, Q., Zhang, G., Zhang, Y. W. Energetics, charge transfer, and magnetism of small molecules physisorbed on phosphorene. *Journal of Physical Chemistry C*, 119(6): 3102–3110, 2015.

[8] Zhao, S., Xue, J., Kang, W. Gas adsorption on MoS_2 monolayer from first-principles calculations. *Chemical Physics Letters*, 595: 35–42, 2014.

[9] Leenaerts, O., Partoens, B., Peeters, F. M. Adsorption of H_2O, NH_3, CO, NO_2, and NO on graphene: a first-principles study. *Physical Review B*, 77(12): 125416, 2008.

[10] Guo, S., Yuan, L., Liu, X., Zhou, W., Song, X., Zhang, S. First-principles study of SO_2 sensors based on phosphorene and its isoelectronic counterparts: GeS, GeSe, SnS, SnSe. *Chemical Physics Letters*, 686: 83–87, 2017.

[11] Abbas, A.N., Liu, B., Chen, L., Ma, Y., Cong, S., Aroonyadet, N., Kopf, M., Nilges, T., Zhou, C. Black phosphorus gas sensors. *ACS nano*, 9(5): 5618–5624, 2015.

[12] Liu, D., Shi, Y., Tao, L., Yan, D., Chen, R., Wang, S. First-principles study of methanol adsorption on heteroatom-doped phosphorene. *Chinese Chemical Letters*, 30(1): 207–210, 2019.

[13] Holzwarth, N. A. W., Tackett, A. R., Matthews, G. E. A Projector Augmented Wave (PAW) code for electronic structure calculations, Part I: atompaw for generating atom-centered functions. *Computer Physics Communications*, 135(3): 329–347, 2001.

[14] Kresse, G., Joubert, D. From ultrasoft pseudopotentials to the projector augmented-wave method. *Physical review b*, 59(3): 1758, 1999.

[15] Evarestov, R. A., Smirnov, V. P. Modification of the Monkhorst-Pack special points meshes in the Brillouin zone for density functional theory and Hartree-Fock calculations. *Physical Review B*, 70(23): 233101, 2004.

[16] Monkhorst, H. J., Pack, J. D. Special points for Brillouin-zone integrations. *Physical review B*, 13(12): 5188, 1976.

[17] Perdew, J. P., Burke, K., Ernzerhof, M. Generalized gradient approximation made simple. *Physical review letters*, 77(18): 3865, 1996.

[18] Giannozzi, P., Baroni, S., Bonini, N., Calandra, M., Car, R., Cavazzoni, C., Ceresoli, D., Chiarotti, G.L., Cococcioni, M., Dabo, I. and Dal Corso, A. QUANTUM ESPRESSO: a modular and open-source software project for quantum simulations of materials. *Journal of physics: Condensed matter*, 21(39): 395502, 2009.

[19] Giannozzi, P., Baroni, S., Bonini, N., Calandra, M., Car, R., Cavazzoni, C., Ceresoli, D., Chiarotti, G.L., Cococcioni, M., Dabo, I., Dal Corso, A. Advanced capabilities for materials modelling with Quantum ESPRESSO. *Journal of physics: Condensed matter*, 29(46): 465901, 2017.

[20] Li, X. B., Guo, P., Cao, T. F., Liu, H., Lau, W. M., Liu, L. M. Structures, stabilities and electronic properties of defects in monolayer black phosphorus. *Scientific reports*, 5(1): 1–11, 2015.

[21] Kaewmaraya, T., Ngamwongwan, L., Moontragoon, P., Karton, A., Hussain, T. Drastic improvement in gas-sensing characteristics of phosphorene nanosheets under vacancy defects and elemental functionalization. *The Journal of Physical Chemistry C*, 122(35): 20186–20193, 2018.

[22] Cai, Y., Ke, Q., Zhang, G., Yakobson, B. I., Zhang, Y.-W. Highly itinerant atomic vacancies in phosphorene. *Journal of the American Chemical Society*, 138(32): 10199–10206, 2016.

[23] Behera, S. K., Deb, P. First principle understanding on electronic and magnetic behaviour in vacancy induced black phosphorous monolayer. In *AIP Conference Proceedings*, volume 2276, pages 020021, 2020, AIP Publishing LLC.

[24] Goulart, L., Fernandes, L. da S., dos Santos, C. L., Rossato, J. Electronic and structural properties of black phosphorene doped with Si, B and N. *Physics Letters A*, 383(32): 125945, 2019.

[25] Safari, F., Moradinasab, M., Fathipour, M., Kosina, H. Adsorption of the NH_3, NO, NO_2, CO_2, and CO gas molecules on blue phosphorene: a first-principles study. *Applied Surface Science*, 464: 153–161, 2019.

[26] Yang, Q., Meng, R.S., Jiang, J.K., Liang, Q.H., Tan, C.J., Cai, M., Sun, X., Yang, D.G., Ren, T.L., Chen, X.P . P. First-Principles Study of Sulfur Dioxide Sensor Based on Phosphorenes. *IEEE Electron Device Letters*, 37(5): 660–662, 2016.

[27] Henkelman, G., Arnaldsson, A., Jónsson, H. A fast and robust algorithm for Bader decomposition of charge density. *Computational Materials Science*, 36(3): 354–360, 2006.

[28] Kokalj, A. Formation and structure of inhibitive molecular film of imidazole on iron surface. *Corrosion Science*, *68*:195-203, 2013.

[29] Chen, G.X., Wang, R.X., Wang, D.D., Li, H.X., Liu, S., Zhang, J.M. First-principles study of CO and NO adsorption on pristine and transition metal doped blue phosphorene. *Vacuum*, 179: 109503, 2020.

[30] Maria, J.P., Nagarajan, V., Chandiramouli, R. Chemosensing nature of black phosphorene nanotube towards $C_{14}H_9Cl_5$ and $C_{10}H_5C_{l7}$ molecules–A first-principles insight. *Computational and Theoretical Chemistry*, 1196: 113109, 2021.